Progress In Electromagnetics Research C, Vol. 107, 245–258, 2021

An Electrically Small 3-D Folded Grounded Loop Antenna for Omnidirectional Connectivity

Harry Contopanagos*

Abstract—Electrically small antennas are of intense and increasing academic and industrial interest due to the advent of ubiquitous RFID devices and more generally within the Internet of Things (IoT) applications. For most of these applications, antennas will have to be as small as possible, when being integrated within a transceiver, while maintaining significant efficiency values. Of particular interest are antennas that can radiate omnidirectionally along a planar surface, thus establishing optimal connectivity capabilities for devices surrounding the corresponding transmitter. Such antennas are important not only for energy harvesting but also for near-field wireless charging applications. In this paper, we report an electrically small antenna of size $ka \approx 0.25$, where a is its effective radius and k the wave vector at operating frequency. The antenna geometry is a 3-dimensional folded meandering loop and contains its own ground, so that it becomes insensitive to the integration environment. The radiation efficiency of the antenna is 70%, and it radiates as a vertically polarized dipole. The operating frequency chosen in this paper targets RFID/IoT applications at 915 MHz, and the impedance matching bandwidth, as realized, is narrow but appropriate for such applications and may be further increased if appropriate matching networks are used.

1. INTRODUCTION

The Internet-of-Things (IoT) is positioned to transform our everyday environment into a network of fully interacting sets of devices communicating with little or no human supervision. In its mature deployment, it will represent the convergence of multiple technologies, including real-time analytics, artificial intelligence, sensing, and other embedded systems. In the consumer space alone, most aspects of the smart home, consumer appliances, automotive and health monitors will be drastically affected. Relevant reports of varying accuracy [1, 2] have estimated the number of IoT devices in the near future to range from 30 to 50 billion and corresponding market value to $7 trillion [3]. McKinsey [4, 5] predicted that the economic impact of IoT can be as high as $11 trillion or about 10% of the world GDP in 2025, but other analyses are more conservative [6, 7]. Regardless of very short-term predictions, associated hype cycles, time-to-market underestimates, and other initial assumptions that affect predictions, there is no doubt that the economic impact of IoT technologies will be very substantial in the near future. From the technologies convergence in IoT, an essential functionality based on corresponding underlying enabling technologies is the wireless connectivity of the devices, especially in the category of short-range wireless which will include the majority of interconnected devices. Antennas and antenna arrays are very important for efficient link budgets in a variety of application segments within this general area, whether they are intended for RFID and related applications [8, 9], Near Field Communications (NFC), Bluetooth Low Energy (BLE), and other enabling technologies and applications [10], even unrelated to data transfer, such as RF Energy Harvesting [11–13] and near-field wireless charging [14].

Received 11 November 2020, Accepted 18 December 2020, Scheduled 24 December 2020
* Corresponding author: Harry Contopanagos (h.contopanagos@inn.demokritos.gr).
The author is with the Institute of Nanoscience and Nanotechnology, National Center for Scientific Research "Demokritos", Agia Paraskevi-Athens 15310, Greece.

IoT connectivity is characterized by transmission of small data volumes and low rates [15], which in turn implies narrow bandwidth requirements, usually of the order of 1 MHz for most applications, and sub-GHz bands, such as 915 MHz in the US and 868 MHz in Europe, are preferred due to the reliable propagation characteristics, especially within home or office environment, where absorption from walls and other fixtures is not detrimental. Antenna form factors for integration in corresponding devices are important [16], especially since many of the interconnected devices will have small size or will be mobile or desktop terminals. Given that the wavelength in these frequencies is fairly large (328–346 mm) and the fact that antennas need to be compact *and* efficient, as well as inexpensive, it becomes obvious that many design challenges need to satisfy all or most of these requirements. In addition, specific deployment characteristics may impose additional constraints relating to the radiation pattern, the device work space, etc.

In this paper, we will present an electrically small antenna, as defined in the general literature, which has inexpensive fabrication, as it uses only stamped metal, while maintaining a radiation efficiency of 70–80%. The electrical size of the antenna is $ka \approx 0.25$–0.28, where k is the free-space wave number at the operation frequency, and a is the effective radius of the antenna, discussed later. One necessity we imposed is that the antenna contains its own ground, so that it becomes insensitive to any device integrated *behind* the antenna. This is usually a very important detail, which is absent on many publications (academic or industrial), which claim small antenna sizes but need large ground planes in order to operate correctly, or match, or obtain the necessary isolation from peripheral device components. A classic example is PIFAs, IFAs, or other folded antennas, which are small antennas requiring large ground planes, in order to obtain both impedance matching and efficient radiation [17–22]. In contrast, in this work the size of the antenna will include its ground, and given that it is a 3-dimensional antenna, the effective radius a we will quote accounts for its size in all 3 dimensions.

The structure of this paper is as follows. In Section 2, we describe the design and layout parameters of the antenna, discuss the electrical size of the antenna and some possible fabrication variants, and present its simulated performance. We further present certain importance performance variations related to key design parameters. In Section 3, we present measurement results and compare them with the corresponding theoretical quantities. Finally, in Section 4 we summarize with brief conclusions. All design simulations in this work were performed with the ANSYS finite-element HFSS full-wave software.

2. DESIGN AND OPTIMIZATION OF THE 3-DIMENSIONAL FOLDED GROUNDED LOOP ANTENNA

In this section, we will analyze the design and optimization of a 3-dimensionally folded loop antenna which contains its own finite ground. The performance targets are that the antenna is electrically small, as defined by the classic Wheeler-Chu analysis [23, 24] and extensive follow-up work relating to the fundamental limits of the radiation quality factor (see for example [25, 26]). A rough estimate of the size of a small antenna is $kR < 1$, where $k = 2\pi/\lambda$ with λ being the free-space wavelength and R the radius of the sphere circumscribing the antenna *including its ground*. More sophisticated current limits relating to small antenna size, impedance matching and radiation efficiency, expanding on previous work [27, 28] can be found in [29–31]. In particular, we can use the volumetrically averaged antenna radius a_V [29], or the 3-D surface averaged antenna radius a_S [31], to characterize more accurately the electrical size of the antenna and quantify its radiation efficiency versus electrical size. According to the volumetrically averaged electrical antenna radius,

$$ka_V = k\left(\frac{V}{4\pi/3}\right)^{1/3} \tag{1}$$

where V is the true geometrical volume of the antenna. If we use the 3-D antenna surface to extract the antenna electrical size, we find instead

$$ka_S = k\left(\frac{\Sigma_j S_j}{4\pi}\right)^{1/2} \tag{2}$$

where S_j is any surface of the 3-D antenna structure. The summation extends over all antenna surfaces, and Eq. (2) provides the effective radius of the corresponding sphere of the same area. Further, the

−10 dB impedance matching band (at a 50-Ohm port) should be a few MHz, as appropriate for IoT and RFID applications, and the radiation pattern should be omnidirectional around the plane of the antenna (the plane of the ground), with vertical polarization relative to that plane. Finally, the antenna should have a maximum radiation efficiency for a fixed small size. We target, as an example, the operation frequency of 915 MHz, which is a band assigned to most IoT devices in the US. Direct scalability to other frequencies is straightforward, especially in this stamped metal realization.

In Fig. 1, we show a 3D isometric view of the design, while in Fig. 2, we show the top view and front view. This design is all laid out in stamped metal, and pure Cu is the metal of choice since it has maximum conductivity. Stamped metal lends itself to inexpensive mass-production, appropriate for industrial implementation, and in the layout of Fig. 1, the antenna and its ground can be fabricated with a planar sheet of stamped metal and then folded. In Fig. 1, M1 is the top antenna layer, M2 the bottom antenna layer, and M3 the antenna ground.

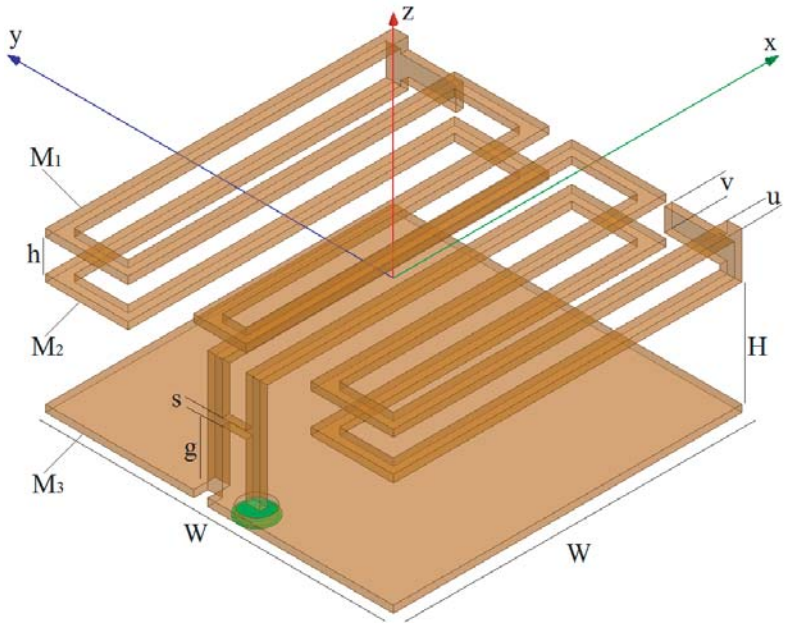

Figure 1. 3-Dimensional isometric view of the antenna layout, containing 3 metal layers.

Obviously, M1 and M2 could also be both included on a double-cladded low-loss dielectric, rather than as two separate free-standing metal layers, with the vertical interconnects between the two layers realized as vertical vias, while the interconnects to the ground are realized as separately soldered metal pins. This, however, would introduce additional dielectric loss and complicate the fabrication, even though it would make the antenna smaller. The feed, indicated by the circular excitation port in Fig. 1, can be practically implemented by an SMA connector whose ground is soldered in the back of the antenna ground M3 and whose signal pin is soldered directly on the signal post of the antenna through the ground hole, as shown in Fig. 3 of the fabricated prototype. In the prototype shown, the ground layer was fabricated separately from the antenna and then soldered.

All the parameters of the optimized design D1 are shown in Table 1, where u is the uniform width of the antenna metal trace; t is the metal thickness common to $M1$, $M2$, and $M3$; and h and H are the spacing between $M1$-$M2$ and $M2$-$M3$ (ground). The size of the antenna is $x \times y \times z = 24 \times 24 \times 11\,\text{mm}^3$, and the diameter of the circumscribing sphere, which is equal to the diagonal of the parallelepiped representing the volume of the antenna, is $2R = 35.68\,\text{mm}$. Hence the geometrically computed electrical size of the antenna at the frequency of operation $f = 915\,\text{MHz}$ ($\lambda = 327.87\,\text{mm}$) is $x \times y \times z = 0.073\lambda \times 0.073\lambda \times 0.033\lambda$ or, using small antenna metrics

$$kR = \frac{2\pi R}{\lambda} = 0.34 \ll 1. \tag{3}$$

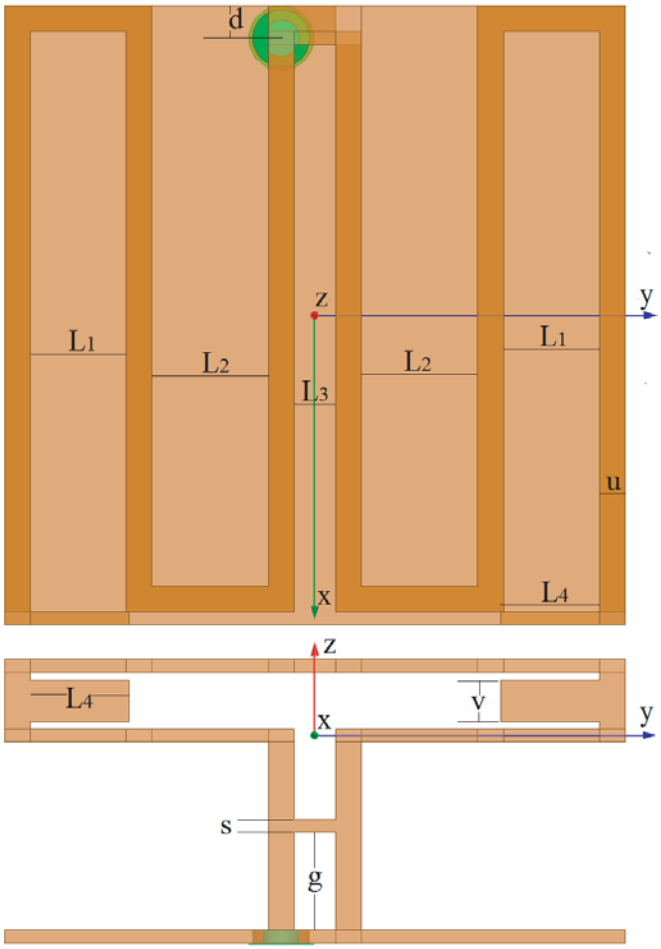

Figure 2. Top view and front view of the antenna layout in true relative scale.

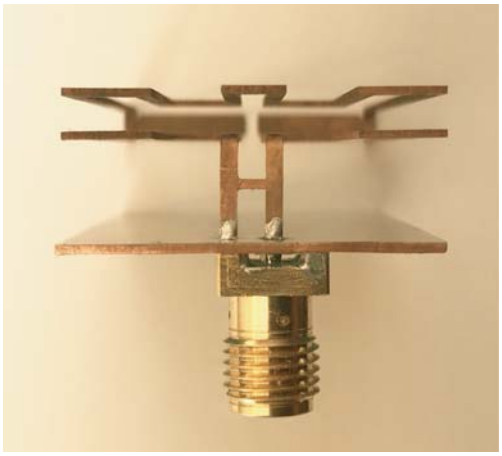

Figure 3. Photograph of the fabricated design D1 showing details of the SMA connector and feed.

According to the more accurate effective sizes of Eqs. (1)–(2),

$$ka_V = \frac{2\pi}{\lambda}\left(\frac{24\times 24\times 11}{4\pi/3}\right)^{1/3}\ \text{mm} = 0.22 \ll 1 \tag{4}$$

Table 1. Layout parameter values (mm) for the antenna designs D1 and D2.

	W	H	h	L_1	L_2	L_3	L_4	d	g	s	u	v	t
D1	24	7.3	2.2	3.7	4.5	1.6	3.8	1.25	3.8	0.5	1	1.6	0.5
D2	25	9.6	2.7	3.9	4.05	1.3	3.8	1.55	5.6	0.5	1.3	2.1	0.5

$$ka_S = \frac{2\pi}{\lambda}\left(\frac{2\times 24\times 24 + 4\times 24\times 11}{4\pi}\right)^{1/2} \text{mm} = 0.25 \ll 1 \tag{5}$$

We note that the effective electrical sizes of Eqs. (4) and (5) are in close agreement, and fairly smaller than the more naive size of Eq. (3), which equates the actual antenna volume with the much larger volume of the circumscribing spherical region, thus overestimating the true radiating volume [23] and corresponding electrical antenna size. The electrical sizes obtained above show that this is quite a small antenna, normalized to its performance that we show later.

Some design, tuning and optimization properties should be noted. First, in Figs. 1 and 2 we observe that we have included a grounding matching stub of width s connecting the signal and ground vertical feeding pins, which is placed a distance g above the ground. This corresponds to a Matching Network (MN) essential for impedance matching. We analyze the need and effect of this matching network with the circuit simulation of Fig. 4. Here, we have simulated the antenna of Figs. 1 and 2 without the matching stub. Then, we imported the simulation result in the form of a touchstone file represented by the box in Fig. 4, and then we cascaded this file with the optimized lumped circuit shown in Fig. 4, consisting of one shunt inductor, one series inductor, and one shunt capacitor after the antenna feed (Port 1).

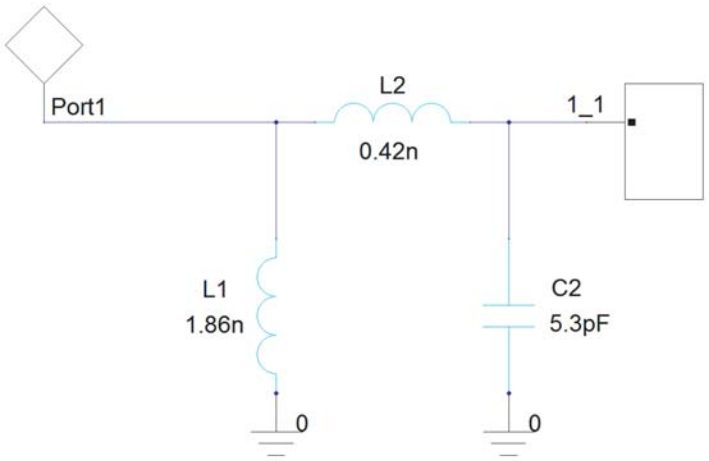

Figure 4. A simple matching network circuit optimization of the antenna without a matching stub.

In Fig. 5, we present simulation results of the antenna complex input impedance without the matching network (curves 1 and 2), with the ideal lumped matching network of Fig. 4 (curves 3 and 4) and with the physical realization of that matching network through the introduction of the matching stub, as shown in the complete design of Figs. 1 and 2.

We note from Fig. 5 that without the matching network, the antenna has a very poor matching, having a resonance at 983 MHz with the impedance value peaking at 4.3 KΩ. With the circuit of Fig. 4, the antenna impedance resonates at 915 MHz, with $Z_{in} \approx 50 + j0\,\Omega$. The antenna with the matching stub of Figs. 1 and 2 produces an input impedance in close agreement with that of the lumped circuit of Fig. 4, matching equally well. Hence, this matching stub is an accurate stamped metal realization of the matching network circuit of Fig. 4, with a minimal layout modification.

Because this is a narrow-band application, it is important to include a simple tuning mechanism for

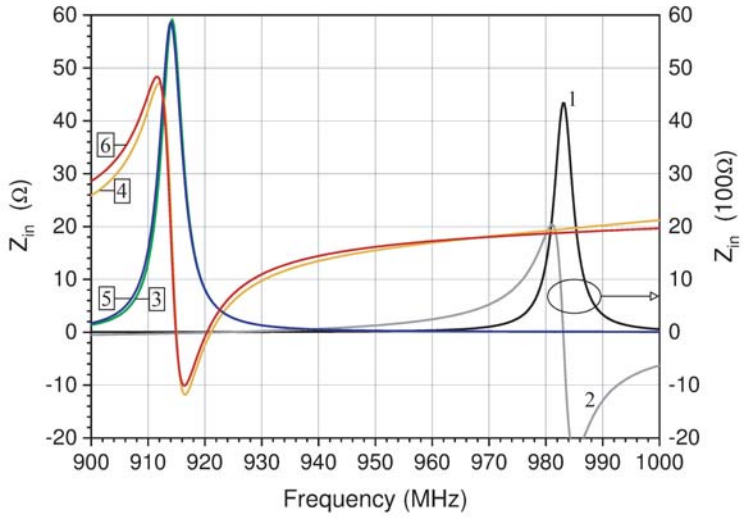

Figure 5. Matching network simulations: Simulated $\mathrm{Re}\{Z_{in}\}$ (curve 1) and $\mathrm{Im}\{Z_{in}\}$ (curve 2), denoted by $Z_{in} = [1] + j[2]$, of the antenna input impedance without the matching stub. Values for these curves are on the right vertical axis of the plot (in units of 100 Ohms); $Z_{in} = [3] + j[4]$ is for the antenna with the lumped MN shown in the circuit of Fig. 4, while $Z_{in} = [5] + j[6]$ is for the complete antenna design with the matching stub shown in Figs. 1, 2. Values for these curves are on the left vertical axis of the plot (in units of Ohms).

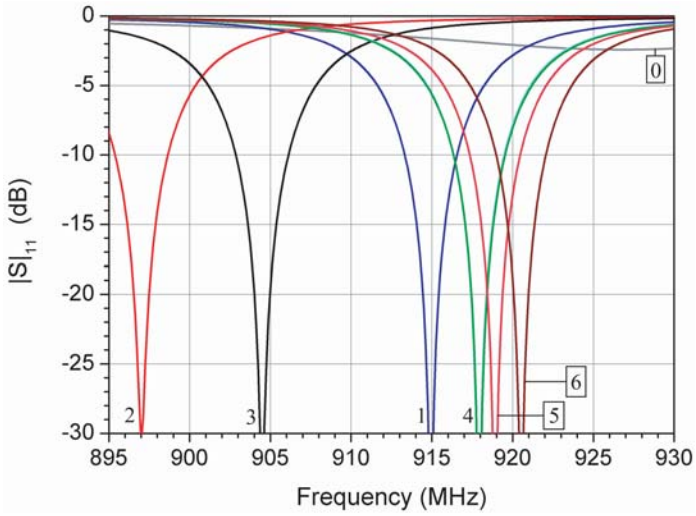

Figure 6. Impedance matching and tuning of the return loss for design D1: [0] Without matching stub, $L_4 = 3.8$ mm; [1] $L_4 = 3.8$ mm; [2] $L_4 = 6.8$ mm; [3] $L_4 = 5.8$ mm; [4] $L_4 = 2.8$ mm; [5] $L_4 = 1.8$ mm; [6] $L_4 = 0.8$ mm.

the fabricated prototype tuning, since dimensional variations in the stamped folded metal prototype and antenna assembly may lead to some antenna detuning. This is achieved by the tuning stubs of length L_4 in Fig. 2, which are included in the stamped metal layout. Fig. 6 presents the frequency variation of the return loss of the antenna for various tuning stub lengths (both stubs have equal lengths), when all other parameters are fixed at the values shown in Table 1. We see that the -10 dB impedance matching bandwidth is 3.5 MHz and that considerable tuning is achieved. Therefore, this is a useful and practical mechanism for prototype fabrication.

Our choice of circuit topology for the matching network in Fig. 4 is motivated by the fact that it is the simplest that reactively loads the antenna and can by physically realized minimally within

the stamped design layout by simply introducing the grounding matching stub of Figs. 1 and 2. For comparison, an even simpler 2-element topology, consisting of a series capacitor and a shunt inductor, can also produce the same matched reflection as shown in Fig. 6. However, the complex impedance of the resulting system is very different from the response $Z_{in} = [3] + j[4]$ of Fig. 5, suggesting that this alternative cannot be physically realized as minimally as our choice of the circuit of Fig. 4.

The simulated total radiation efficiency of the antenna design D1 is quite high at 70% as shown in Fig. 7, flat over a much broader frequency band than the impedance matching band shown in Fig. 6. We point out that the efficiency for design D1 remains the same regardless of all variations of Fig. 6, i.e., regardless of tuning or whether we include or not the matching stub. Since the radiating bandwidth of the antenna is much larger than the impedance bandwidth achieved in this design implementation, it is possible that the impedance matching bandwidth can be increased relative to the present implementation, within the high-efficiency band of the antenna, by more complicated matching networks, if more broadband operation is desired, see for example [22, 32, 33]. We will present such a study with the associated quality factors and their comparison to fundamental small-antenna limits in a future publication.

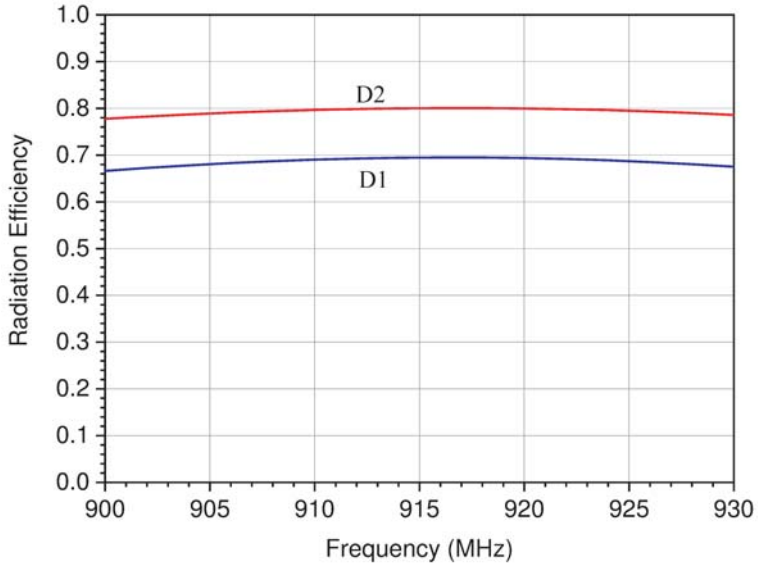

Figure 7. Radiation efficiency for designs D1 and D2.

Regarding the overall choice of the design parameters of D1, the size W of the antenna and ground was chosen as the minimum size where the antenna meandering trace length on $M1$ and $M2$ could achieve the resonant frequency desired, given the overall system height, fixed at 11 mm. This requirement also produced the trace width u to be around 1 mm. Given the prescribed antenna area, the meanders on $M1$ and $M2$ should be spaced approximately evenly on the planar area, in order to produce good impedance matching and also maximize efficiency. Otherwise, if the meanders were too dissimilar (L_1 or L_2 were too small), additional tuning would be required by further increasing the length L_4 of the tuning stubs, but the tuning range would be limited, and the efficiency of the resulting tuned design would be lower. For example, with L_1 smaller than the value in Table 1 by 1 mm and therefore L_2 larger by 1 mm, the antenna would be tuned to a frequency $f_0 = 923$ MHz, and the tuning stubs would have to be a full 4 mm longer, i.e., $L_4 = 7.8$ mm, to tune the antenna down to 915 MHz. Even then, the resulting tuned antenna efficiency would be 68%, smaller than the efficiency achieved by the optimized design D1. Further, the tuning stub length range would now be limited for actual prototype tuning. If L_1 was smaller by 2 mm, then $f_0 = 948$ MHz, and there would not be sufficient length margins for the tuning stubs to tune the antenna down. The best one could do is to have tuning stubs of length $L_4 = 10.8$ mm, which would tune the antenna to $f_0 = 938$ MHz, with a resulting efficiency of 66%. Inversely, if L_1 was larger by 1 mm than the value in Table 1, with L_2 smaller by the same amount, the results would be

the same as in the previous corresponding case. With L_1 larger by 2 mm, $f_0 = 938$ MHz, and there are still not sufficient length margins for the tuning stubs to tune the antenna down. The best one could do, with $L_4 = 10.8$ mm, is to reach $f_0 = 926$ MHz, with a resulting efficiency of 67%. Hence, the precise design values of the optimized lengths L_1, L_2, and L_4 of D1 in Table 1 were determined through numerical optimization of impedance matching and efficiency. A similar behavior follows the choice of the tuning stub width v, where narrower stubs would tune the antenna up, and then longer stub lengths would have to be used to tune it down, with a modest reduction in efficiency. Combined effects of the overall design parameter space are demonstrated below, as we explore an alternative design D2.

A significant variance of the radiation efficiency is achieved by altering other design parameters of the antenna. To gain a sense of the performance sensitivity regarding efficiency (and therefore corresponding gain), we include in Fig. 7 total radiation efficiency curves for the two different designs, D1 and D2, where all relevant parameters are shown in Table 1.

We observe that the total efficiency for design D2 is 80%, superior to that of D1 (a 14% efficiency increase). A similar increase is obtained for the impedance matching bandwidth which is now at 4.5 MHz. The important parameters achieving this are the larger values of the spacings H, h and the larger value of the trace width u. Of course, the antenna volume for design D2 is larger, at $x \times y \times z = 25 \times 25 \times 13.8\,\text{mm}^3$. This is a 36% increase in volume or about 9–11% increase in electrical size (depending on whether we use of Eq. (2) or (1), respectively). The efficiencies of designs D1 and D2, compared to their corresponding electrical sizes obtained from Eqs. (4)–(5), show that this antenna's performance is close to the best published limits [29, 30].

In Fig. 8, we show the 3-dimensional polar plot of the simulated antenna gain for design D1, for the same axes orientation as in Fig. 1. We see that the antenna has a perfect dipole radiation pattern, with maximum gain at 0 dBi; therefore, it is a perfectly omnidirectional dipole antenna. The antenna is vertically polarized, and it behaves in all respects as a dipole perpendicular to the antenna ground, even though the antenna is fed as a grounded loop and not as a differentially fed antenna (typical dipole or loop feeds). This radiation pattern is ideal for omnidirectionally linked devices residing randomly on a planar surface, such as a table. It is important to notice here that the antenna can be quite close to that surface and yet not affected by the material of the surface, even when that is metal, because it is grounded and therefore shielded. This is not true for other small antennas, such as 2-dimensionally folded dipoles, which typically cannot be shielded by including a nearby ground, since this would short the antenna due to images induced by the nearby ground that would cancel the antenna currents. Instead, this antenna is not shorted despite the existence of its ground very near its structure.

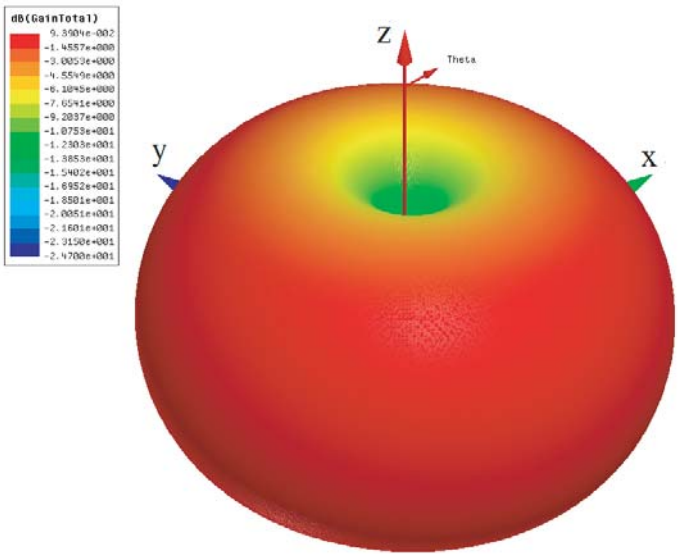

Figure 8. Total antenna gain (in dBi) at 915 MHz. The gain is due exclusively to the $\hat{\theta}$ component of the electric field (vertical polarization at $\theta = 90°$), with the cross-polarization (horizontal polarization) smaller by 25 dB.

3. MEASUREMENTS AND VALIDATION

A stamped metal prototype antenna, shown in Fig. 3, was fabricated according to the parameters of Table 1, except for the stub length, which was retained much longer for tuning purposes. The stubs were then clipped by small steps while the return loss is continuously measured through a vector network analyzer, to achieve measured tuning at 915 MHz. The metal used in the fabrication was pure copper, in order to maximize the antenna performance, as also used in the design and optimization of the previous section. Regarding the fabricated prototype, the concept behind the design of Fig. 1 is that it can be fabricated with a single stamped metal sheet, including the ground and then folded as indicated, to produce the grounded antenna structure. This is why a square notch appears in Fig. 1 on the ground pin of the antenna, which indicates folding. The round hole on the ground, through which the signal pin passes, is not necessary and can be substituted by a square notch surrounding the folded signal pin on 3 sides so that the signal post can also be folded, landing in the middle of that square notch without touching the ground, without any change in the antenna response. For the actual fabricated prototype, the antenna with the feed was fabricated by stamped metal and folded in a commercial facility. Then, in-house, the ground was cut separately, the feed hole was drilled, and the connector was soldered first on the back of the ground with its signal pin centered. Then the antenna ground and signal pins were also soldered appropriately, as shown in the photograph of Fig. 3. During prototype assembly, a plastic spacer of appropriate thickness was used to ensure antenna planarity and parallel orientation to the ground at the precise design height H. Because of the significant thickness of the folded metal trace (0.5 mm) relative to overall antenna dimensions, the prototype was mechanically quite robust. In Fig. 9, we compare the theoretical versus the measured return loss of the antenna. We should mention that we had to adjust the length of the tuning stubs in Table 1, in order to perfectly match the fabricated antenna at the intended operating frequency, since the antenna is inherently narrowband. This mechanism offsets fabrication inaccuracies, provided that these variances are small. For the fabrication at hand, the tuning stubs had to be 13% longer than their design value on Table 1, i.e., their length was 4.3 mm. With this minor tuning, we observe that the measured return loss is in good agreement with the simulated one. The -10 dB impedance matching bandwidth of the antenna is measured at about 5.7 MHz, larger than the simulated one which is 3.5 MHz. Fabrication inaccuracies, surface roughness, as well as other distributed parasitic matching effects may cause this difference. As mentioned in the introduction, this bandwidth is sufficient for the intended IoT applications of this class of antennas.

In Figs. 10 and 11, we compare the total gain of the antenna measured in an anechoic chamber with the corresponding simulated quantity, at 915 MHz, for the two principal cuts of the 3-dimensional

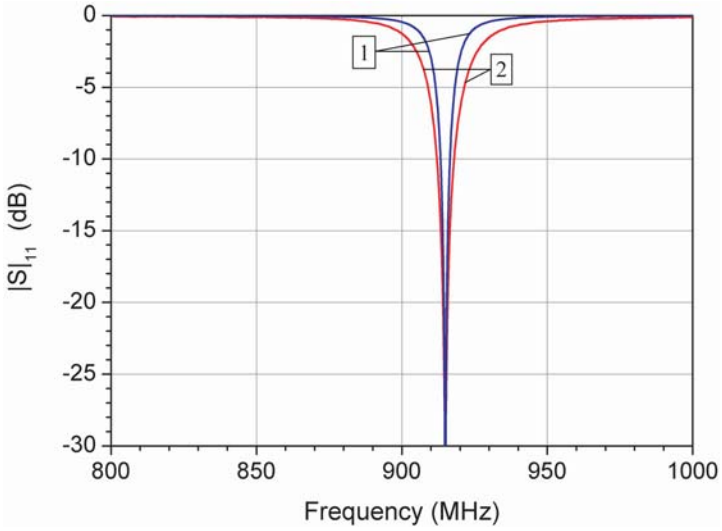

Figure 9. Theoretical (curve [1]) vs. measured (curve [2]) return loss for the antenna design D1.

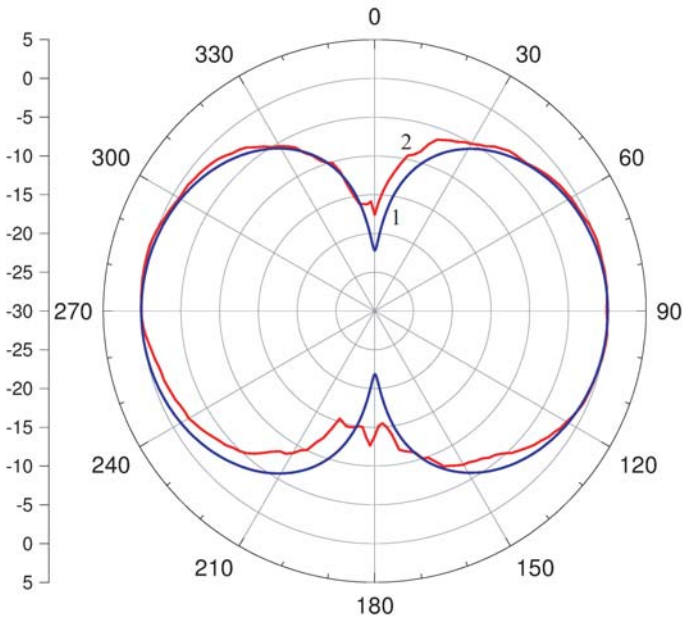

Figure 10. Theoretical [1] vs. measured [2] gains at 915 MHz on the $[yz]$ plane for the antenna design D1.

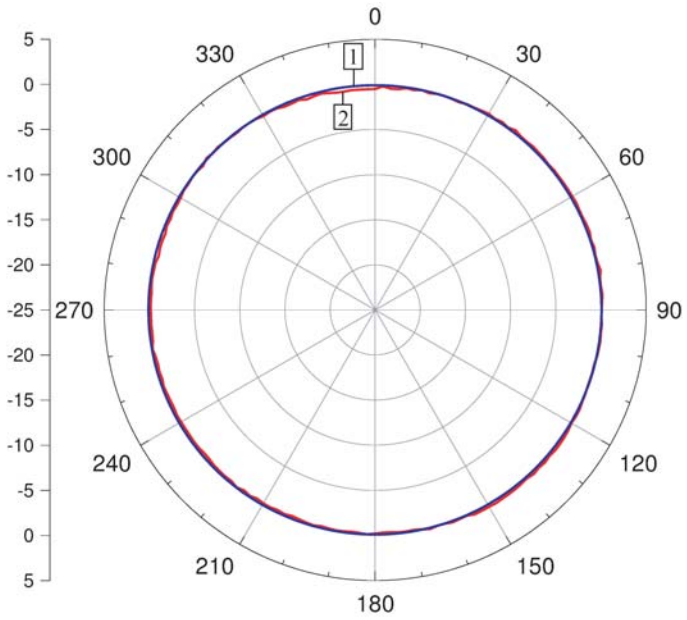

Figure 11. Theoretical [1] vs. measured [2] gains at 915 MHz on the $[xy]$ plane for the antenna design D1.

radiation pattern shown in Fig. 8. Fig. 10 is the cut on the $[yz]$ plane, i.e., it is the function $G_{TOT}(\theta, \phi = 90°)$, while Fig. 11 shows the corresponding comparison for the cut on the $[xy]$ plane, hence it plots the function $G_{TOT}(\theta = 90°, \phi)$.

Both measurements are in excellent agreement with the corresponding theoretical simulations and show an antenna radiating omnidirectionally as a dipole perpendicular to the $[xy]$ plane, with a 0 dBi gain. We also note that the measured and theoretical gains due to the horizontal component of the electric field (the component parallel to the $[xy]$ plane) are completely negligible, and the total gain

plotted is due to the vertical component of the electric field. The antenna therefore acts as a dipole, completely linearly polarized and with vertical polarization relative to the plane of the antenna.

In Fig. 12, we show the maximum antenna gain versus frequency, around the central resonant frequency. Again, very good agreement is observed between simulations and measurements, within the common impedance matching band of Fig. 9. We note here that the plotted measured and simulated gains are the realized gains, which include the return loss of Fig. 9. Outside the common matching bands, the measured realized gain is considerably higher than the simulated one, simply because the measured return loss is smaller than the simulated one, and therefore less power is reflected back to the feed in the measured antenna than in the theoretical one, for these frequencies. We also note that the excellent agreement of the maximum gain values near the resonant frequency validates the theoretical radiation efficiency of the antenna, found to be 70% in Fig. 7.

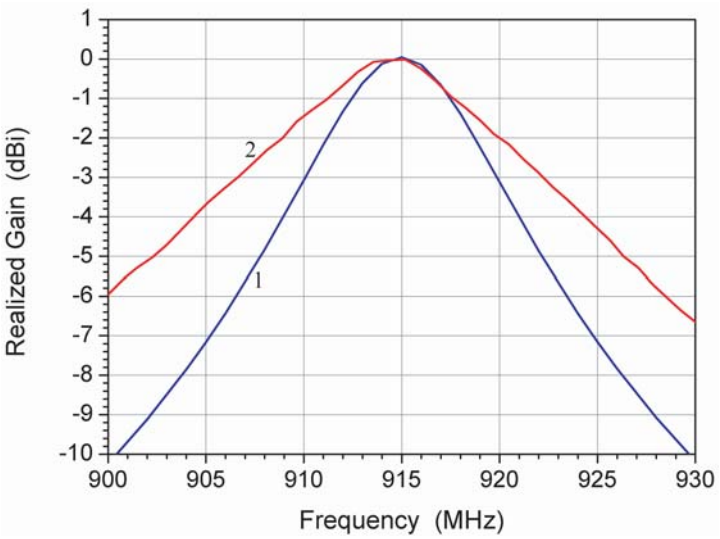

Figure 12. Theoretical [1] vs. measured [2] maximum realized gains (in dBi) vs. frequency for antenna design D1.

It is interesting to compare the characteristics and performance of this antenna to alternative designs existing in the recent literature. We summarize this comparison in Table 2. The electrical size ka_S for all antennas in this table is computed from Eq. (2), which is appropriate for both planar and 3D antennas.

Table 2. Comparison with relevant previous work: f_0 is the frequency of operation, Z_{in} BW is the impedance matching bandwidth at -10 dB, while efficiencies (Eff.) and realized gains (R. Gain) are included when available.

	Antenna Type	Dimensions (mm)	f_0 (MHz)	Eff.	R. Gain	Z_{in} BW (MHz)	ka_S
This work	3D	$24 \times 24 \times 11$	915	70%	0 dBi	5.7	0.25
Ref. [32]	3D	$43.5 \times 28.5 \times 11$	915	47%	-0.6 dBi	26.4	0.34
Ref. [33]	Planar	46×37	1000	N/A	-3.8 dBi	15	0.39
Ref. [15]	Planar	25×40	915	25%	N/A	N/A	0.17
Ref. [8]	Planar	31×31	922	N/A	-4.4 dBi	13.5	0.18
Ref. [9]	Planar CP	62×62	915	N/A	-0.2 dBi (2.8 dBic)	22	0.34

From the above antennas, only the IFA of [15] and the folded dipole-loop printed on a double-cladded PCB of [8] are effectively smaller than the present one, even though they both occupy a larger area, because they are planar. However, the efficiency of [15] is one third of the efficiency presented in this work, while the gain of [8] is 4.4 dB lower than the present antenna (indicating a proportionally lower efficiency). All the other antennas are substantially larger and of lower efficiency or gain. The planar antennas in Table 2 have an additional disadvantage since they do not have a shielding ground, as the present one does. Perhaps the most direct comparison is with the 3D antenna of [32], which is substantially larger and of lower efficiency, but substantially more broadband. The antenna in [9] is circularly polarized (CP), and we include it mainly for size comparison. In conclusion, the present antenna is advantageous to prior designs presented in Table 2, with respect to size/efficiency characteristics. It is however more narrowband (with the exception of the antenna in [15] which does not match at the −10 dB level).

A final note relating these results to the impedance matching bandwidth of the antenna as designed and measured is worth repeating. It is clear from the efficiency plot of Fig. 7 that the antenna radiates efficiently in a wider frequency band than the one constrained by the impedance bandwidth. Hence, if a more broadband operation is desired, it should be possible to obtain a version of this antenna that will efficiently radiate in wider band, provided that an appropriate low-loss (ideally reactive) matching network is designed and implemented at the antenna feed, in order to increase the current impedance bandwidth.

4. CONCLUSIONS

In this paper, a novel very small antenna has been designed and fabricated using exclusively stamped metal. The antenna as implemented has targeted IoT/RFID applications at the 915 MHz frequency band, but is readily scalable to other operation bands. The basic design requirements that have been successfully met are that the antenna has a very small electrical size, yet maintains very high radiation efficiency at the level of 70%–80%, and further it radiates omnidirectionally on the horizon. The stamped metal design makes it particularly inexpensive for industrial fabrication. The antenna is a grounded, 3-dimensionally folded loop with an integrated matching network, all implemented in stamped metal. Theoretical simulations and measurements are in general in very good agreement, and validate the design, thus making this antenna a proper candidate for industrial IoT applications where size, cost, high efficiency, and omnidirectional device link between a variety of devices, in particular when being spatially distributed on the same planar surface, is desired. In the future, we will perform a detailed study of the maximum impedance matching bandwidth of this antenna in relation to the resulting quality factors and their theoretical minimum limits for small antennas, using a variety of more complicated reactive matching networks.

REFERENCES

1. Evans, D., "The internet of things: How the next evolution of the internet is changing everything," Cisco Internet Business Solutions Group (IBSG), Cisco Systems, Inc., San Jose, CA, White Paper [Online] http://www.cisco.com/web/about/ac79/docs/innov/IoT_IBSG_0411FINAL.pdf, 2011.
2. Nordrum, A., "Popular Internet of Things forecast of 50 billion devices by 2020 is outdated," *IEEE Spectrum* [Online] https://spectrum.ieee.org/tech-talk/telecom/internet/popular-internet-of-things-forecast-of-50-billion-devices-by-2020-is-outdated, 2016.
3. Hsua, C. L. and J. Chuan-Chuan Lin, "An empirical examination of consumer adoption of Internet of Things services: Network externalities and concern for information privacy perspectives," *Comp. Human Behavior*, Vol. 62, 516–527, 2016.
4. Manyika, J., et al., "Unlocking the potential of the Internet of Things," McKinsey Global Institute, McKinsey & Company (Digital) [Online] https://www.mckinsey.com/industries/semiconductors/our-insights/whats-new-with-the-internet-of-things#, 2015.

5. Patel, M., J. Shangkuan, and C. Thomas, "What's new with the Internet of Things?" McKinsey & Company (Semiconductors) [Online] https://www.mckinsey.com/industries/semiconductors/our-insights/whats-new-with-the-internet-of-things#, 2017.
6. Edquist, H., P. Goodridge, and J. Haskel, "The internet of things and economic growth in a panel of countries," *Econ. Innov. New Technology*, [Online] https://doi.org/10.1080/10438599.2019.1695941, 2019.
7. Espinoza, H., et al., "Estimating the impact of the internet of things on productivity in Europe," *Heliyon*, Vol. 6, e03935 [Online] https://doi.org/10.1016/j.heliyon.2020.e03935, 2020.
8. Lai, X., Z. Xie, and X. Cen, "Compact loop antenna for near-field and far-field UHF RFID applications," *Progress In Electromagnetics Research*, Vol. 37, 171–182, 2013.
9. Bhaskar, S. and A. K. Singh, "Meandered cross-shaped slot circularly polarised antenna for handheld UHF RFID reader," *Int. J. Electron. Commun. (AEU)*, Vol. 100, 106–113, 2019.
10. Damis, H. A., et al., "Investigation of epidermal loop antennas for biotelemetry IoT applications," *IEEE Access*, Vol. 6, 15806–15815, 2018.
11. Contopanagos, H. F., P. Broutas, and S. Chatzandroulis, "Embedded multi-slotted PIFAs for remotely powered passive UHF RFID tags," *Microw. Opt. Tech. Lett.*, Vol. 54, No. 10, 2379–2383, 2012.
12. Broutas, P., et al., "A RF power harvester with integrated antenna capable of operating near ground planes," *Sensors and Actuators A*, Vol. 186, 284–288, 2012.
13. Mohammadpour-Aghdam, K., et al., "Miniaturized integrated antennas for far-field wireless powering," *Int. J. Electron. Commun. (AEU)*, Vol. 66, No. 10, 789–796, 2012.
14. Hu, C. H., et al., "One- and two-dimensional antenna arrays for Microwave Wireless Power Transfer (MWPT) systems," *IEEE Wireless Power Transfer Conf. (WPTC)*, 1–4, Taipei, Taiwan, May 10–12, 2017.
15. Lizzi, L., et al., "Design of Miniature Antennas for IoT Applications," *IEEE 6th Int. Conf. on Comm. Electr. (ICCE)*, 234–237, 2016.
16. Lizzi, L. and F. Ferrero, "Use of ultra-narrow band miniature antennas for internet-of-things applications," *Electron. Lett.*, Vol. 51, No. 24, 1964–1966, 2015.
17. Powell, C. R. and R. D. Murch, "A capacitively loaded PIFA for compact mobile telephone handsets," *IEEE Trans. Antennas Propag.*, Vol. 45, No. 5, 837–841, 1997.
18. Liu, Z. D., P. S. Hall, and D. Wake, "Dual-frequency planar inverted-F antenna," *IEEE Trans. Antennas Propag.*, Vol. 45, No. 10, 1451–1458, 1997.
19. Virga, K. L. and Y. Rahmat-Samii, "Low profile enhanced-bandwidth PIFA antennas for wireless communications packaging," *IEEE Trans. Antennas Propag.*, Vol. 45, No. 10, 1879–1888, 1997.
20. Salonen, P., M. Keskilammi, and M. Kivikoski, "Single-feed dual-band inverted-F antenna with U-shaped slot," *IEEE Trans. Antennas Propag.*, Vol. 48, No. 8, 1262–1264, 2000.
21. Contopanagos, H., S. Rawson, and L. Desclos, "Wheeler's law and related issues in integrated antennas," *IEEE AP-S Digest*, 2055–2058, Monterey, CA, 2004.
22. Dong, Y., J. Choi, and T. Itoh, "Folded strip/slot antenna with extended bandwidth for WLAN application," *IEEE Ant. Wireless Propag. Lett.*, Vol. 16, 673–676, 2017.
23. Wheeler, H. A., "Fundamental limitations of small antennas," *Proc. IRE*, Vol. 35, No. 12, 1479–1484, 1947.
24. Chu, L. J., "Physical limitations of omni-directional antennas," *J. Appl. Phys.*, Vol. 19, No. 12, 1163–1175, 1948.
25. McLean, J. S., "A re-examination of the fundamental limits on the radiation Q of electrically small antennas," *IEEE Trans. Antennas Propag.*, Vol. 44, No. 5, 672–676, 1996.
26. Sten, J. C., P. K. Koivisto, and A. Hujanen, "Limitations for the radiation Q of a small antenna enclosed in a spheroidal volume: Axial Polarization," *Int. J. Electron. Commun. (AEU)*, Vol. 55, No. 3, 198–204, 2001.
27. Best, S. R., "Low-Q electrically small linear and elliptical polarized spherical dipole antennas," *IEEE Trans. Antennas Propag.*, Vol. 53, No. 3, 1047–1053, 2005.

28. Kim, O. S., "Low-Q electrically small spherical magnetic dipole antennas," *IEEE Trans. Antennas Propag.*, Vol. 58, No. 7, 2210–2217, 2010.
29. Pfeiffer, C., "Fundamental efficiency limits for small metallic antennas," *IEEE Trans. Antennas Propag.*, Vol. 65, No. 4, 1642–1650, 2017.
30. Thal, Jr., H. L., "Radiation efficiency limits for elementary antenna shapes," *IEEE Trans. Antennas Propag.*, Vol. 66, No. 5, 2179–2187, 2018.
31. Shahpari, M. and D. V. Thiel, "Fundamental limitations for antenna radiation efficiency," *IEEE Trans. Antennas Propag.*, Vol. 66, No. 8, 3894–3901, 2018.
32. Kumar, S., et al., "A bandwidth enhanced 915 MHz antenna for IoT wrist-watch applications," *13th European Conf. Ant. Propag. (EuCAP 2019)*, 1–5, Krakow, Poland, March 31–April 5, 2019.
33. Das, S., et al., "A strongly miniaturized and inherently matched folded dipole antenna for narrowband applications," *IEEE Trans. Antennas Propag.*, Vol. 68, No. 5, 3377–3386, 2020.